Journal of ELECTRONIC MATERIALS, Vol. 43, No. 6, 2014
DOI: 10.1007/s11664-014-3000-1
© 2014 TMS

# Analysis of the Microstructure of $Mg_2Si$ Thermoelectric Devices

SHIGEYUKI NAKAMURA,[1,3] YOSHIHISA MORI,[2]
and KEN'ICHI TAKARABE[2]

1.—Tsuyama National College of Technology, 624-1 Numa, Tsuyama 708-8509, Japan. 2.—Okayama University of Science, 1-1 Ridaicho, Okayama 700-0005, Japan. 3.—e-mail: nakamura@tsuyama-ct.ac.jp

High-performance $Mg_2Si$ thermoelectric devices have been obtained by spark plasma sintering of high-purity, pre-synthesized, all-molten $Mg_2Si$ powder. We studied the effects of source powder particle size on thermoelectric performance. To improve the performance, further investigation of the microstructure of the devices is needed. In this work we studied the microstructure of grain boundaries and interfaces between electrodes and $Mg_2Si$ sintered bodies to increase understanding of $Mg_2Si$ thermoelectric devices.

**Key words:** $Mg_2Si$, contact resistivity, interface, grain boundary

## INTRODUCTION

There has recently been an increase in research on, and development of, thermoelectric devices to overcome global warming and depletion of energy resources.[1] However, these devices require further investigation in terms of conversion efficiency and economic potential. Although commercially available Pb–Te and Bi–Te-based thermoelectric devices have high figures of merit, they contain toxic and rare elements.[2] In contrast, $Mg_2Si$ is regarded an environment-friendly candidate for thermoelectric devices because it contains nontoxic and abundant elements.[3–10] High-performance $Mg_2Si$ thermoelectric devices have been obtained by spark plasma sintering (SPS) of high-purity, pre-synthesized, all-molten $Mg_2Si$ powder.[11] We studied grain size during sintering and did not observe grain growth if the particle-size distribution of the starting powder was relatively uniform; grain growth was observed if the distribution was relatively nonuniform.[12,13] To improve the performance of the devices, further investigation of the devices is required, for example oxide presence at the grain boundaries and electrical properties of the interface between electrodes and the $Mg_2Si$ bulk. In this paper we report results from analysis of the microstructure of grain boundaries and interfaces between electrodes and bulk $Mg_2Si$ performed to enable better understanding of $Mg_2Si$ thermoelectric devices. Electric resistance is very important, because this substantially affects thermoelectric output power. To reduce the contact resistance of devices, we investigated use of new electrodes fabricated by different methods. Results from electrode fabrication are also reported.

(Received June 22, 2013; accepted January 3, 2014;
published online January 31, 2014)

## EXPERIMENTS

$Mg_2Si$ thermoelectric devices used in this study were prepared as follows. Commercially available, high purity, pre-synthesized, all-molten, polycrystalline Al-doped $Mg_2Si$ chunks (purchased from Yasunaga, Japan) were milled into powder of average diameter 45–75 $\mu$m. The $Mg_2Si$ powder was then sintered with SPS equipment (SPS-820S; SPS Sintech, Japan) into cylindrical solids and these were cut into quadrangular prisms, $4 \times 4 \times 7$ mm$^3$ in size, for fabrication of the thermoelectric devices. Nickel electrodes were fabricated on the both sides of the devices by simultaneous sintering, with and without a buffer layer, of a mixture of Ni and $Mg_2Si$ powders, by thermal spraying, by post sintering with an Ni plate, and by sputtering. Seebeck coefficient and electrical conductivity were measured by use of a ZEM-3 (Ulvac Riko, Japan) from 100°C to 600°C with a temperature difference of 30°C. Devices were studied with a scanning electron microscope (SEM; JSM-6510; Jeol, Japan), to observe surface morphology, and with an energy-dispersive x-ray spectroscope (EDX; JED-2300; Jeol), for qualitative analysis. Microstructural

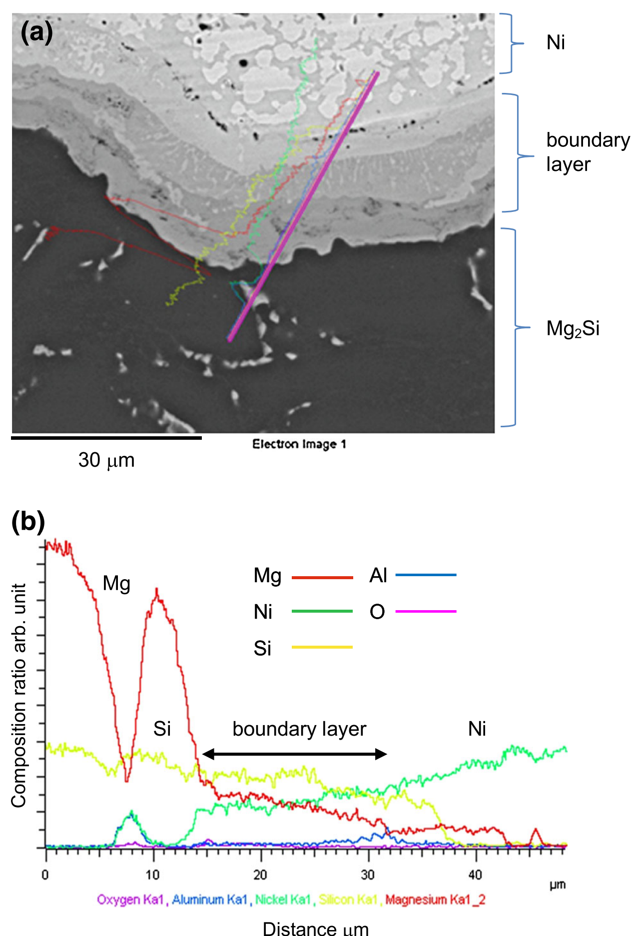


Fig. 1. SEM image (a) and result of EDX line scan (b) of interface of Ni electrode and $Mg_2Si$ sintered body. A boundary layer consisting of Ni, Si, and Mg is present between the Ni electrode and the $Mg_2Si$ sintered body.

electrical resistivity was measured by use of two point probes equipped in SEM at a measurement voltage of 5 mV. The total electrical resistance of devices and electrical resistance of $Mg_2Si$ sintered bodies were measured by use of the four-probe method. Contact resistance was calculated by subtracting the electrical resistance of the $Mg_2Si$ sintered body from the total resistance.

## RESULTS AND DISCUSSION

First, we investigated the interface between electrode and $Mg_2Si$ sintered body. Figure 1a shows a SEM image of the interface. In Fig. 1a, the upper white area is the Ni electrode and the lower black area is the $Mg_2Si$ sintered body. Between these areas, we can see the boundary layer whose contrast is different from those of both the Ni area and the $Mg_2Si$ area. We then determined elemental composition by use of EDX line scan; Fig. 1b shows the result obtained along the red line in Fig. 1a from the $Mg_2Si$ sintered body to the Ni electrode. In Fig. 1b,

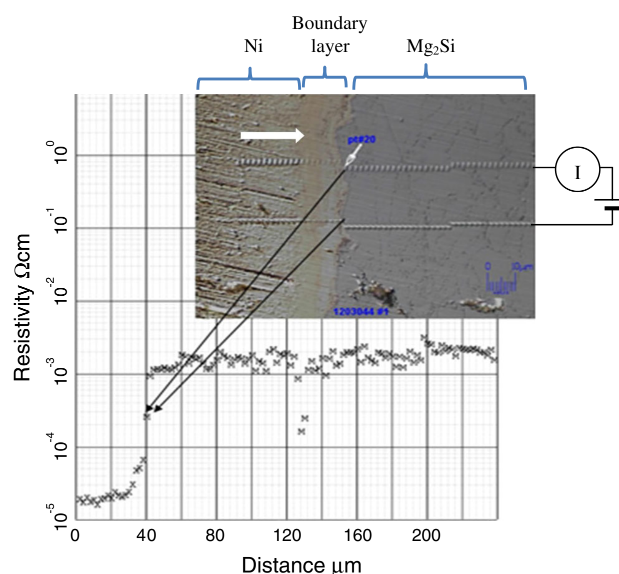


Fig. 2. Electrical resistivity measured every 2 μm from the electrode to the $Mg_2Si$ bulk through the boundary layer. A bold white arrow denotes the scan direction of the probes. SEM image inset. M and X denote $Mg_2Si$ and Ni, respectively.

from approximately 13 μm to approximately 33 μm, the area consists of Mg, Si, and Ni; we can therefore conclude the boundary layer is composed of these three elements. To clarify the effects of the boundary layer on contact resistance, we measured the microstructural resistivity of the boundary layer. Electrical resistivity was measured every 2 μm from the electrode to the $Mg_2Si$ sintered body via the boundary layer. A voltage of 5 mV was applied between the upper and lower probes. Figure 2 shows the results from resistivity measurement, with the measurement points. We can clearly see the traces marked by probes in the SEM image. In the boundary layer, the resistivity gradually increases then rises substantially at the interface between the boundary layer and the $Mg_2Si$ sintered body. The resistivity of the boundary layer is almost same as that of the electrode, so this gradual increase seems to have no effect on contact resistance. The intermediate layer between the Ni electrode and the $Mg_2Si$ is also known to reduce the contact resistance, and was patented by Iida et al.[14]

Second, we investigated the grain boundaries of the sintered $Mg_2Si$ body. Figure 3 shows an SEM image and EDX maps of the sintered sample. Precipitates composed of Mg and O were observed, suggesting the presence of MgO. To clarify the origin of the MgO we examined the starting $Mg_2Si$ chunks by SEM and EDX before sintering. Figure 4 shows an SEM image and EDX maps of the chunks before sintering. We did not observe MgO or other oxides in the chunks, even for areas larger than that of the sintered $Mg_2Si$ bulk, but Al precipitates were observed. This suggests the origin of MgO is not the starting material but that oxygen is present during

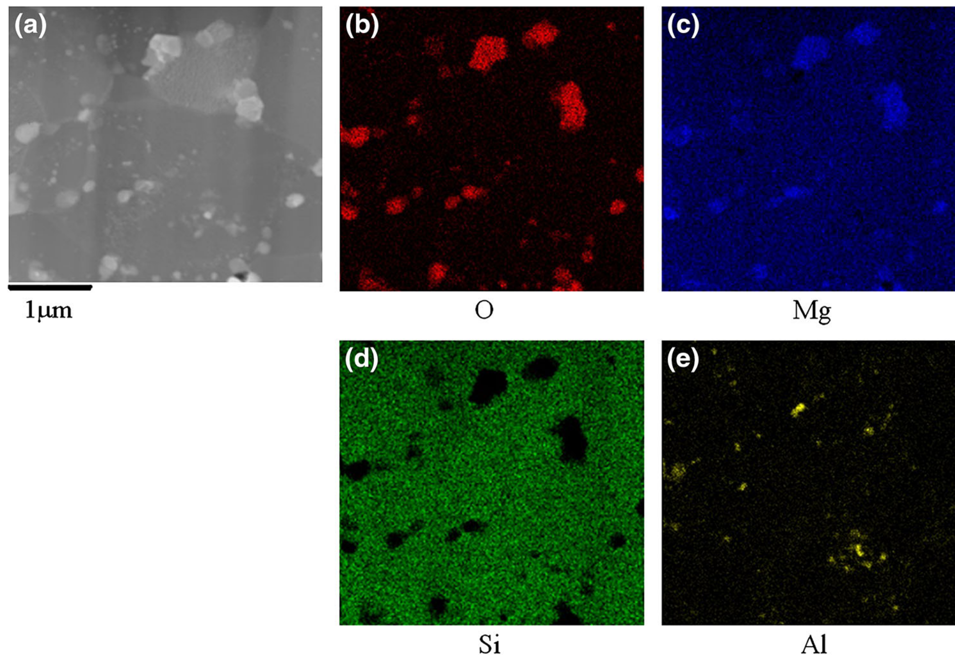


Fig. 3. EDX maps of $Mg_2Si$ sintered body: (a) SEM image of the area analyzed; (b) oxygen; (c) magnesium; (d) silicon; (e) aluminium.

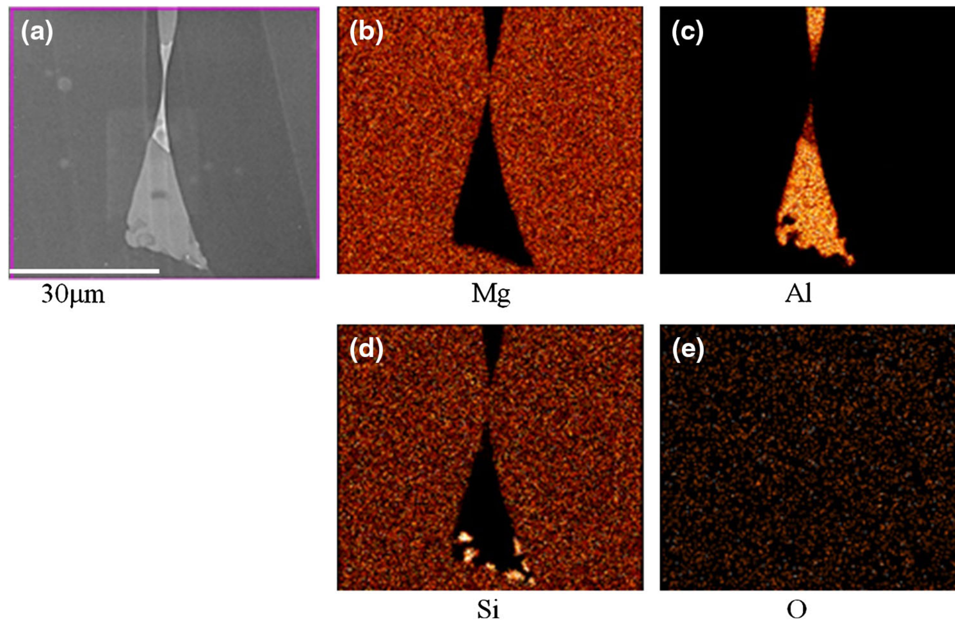


Fig. 4. EDX maps of high-purity, pre-synthesized, all-molten Al-doped $Mg_2Si$ chunk: (a) SEM image of the area analyzed; (b) magnesium; (c) aluminium; (d) silicon; (e) oxygen.

sintering. Synthesis without reaction with oxygen is preferred to avoid MgO formation.

Finally, we attempted to develop electrode fabrication methods. Electrodes have usually been fabricated by simultaneous sintering—$Mg_2Si$ powder and nickel powder at both sides of the $Mg_2Si$ are sintered simultaneously. Electrodes with a buffer layer were also fabricated. The buffer layer is a mixture of Ni and $Mg_2Si$ powders. The mixed powder is placed between Ni and $Mg_2Si$ powder and then sintered. Electrodes were also fabricated by thermal spraying, post sintering, and sputtering. For the thermal spraying, Ni was sprayed on to both sides of an $Mg_2Si$ sintered body at an Ar pressure of 100 Torr, plasma power of 26 kW, and distance from nozzle to a sample of 200 mm. For post sintering, Ni plates placed on both sides of the $Mg_2Si$ sintered body were sintered by SPS. For

**Table I. Summary of the electric resistance of devices with electrodes prepared by different methods**

| Method | Resistance (mΩ) Entire | $Mg_2Si$ only | Contact |
|---|---|---|---|
| Simultaneous sintering without a buffer layer | 6.21 | 4.10 | 2.11 |
| Simultaneous sintering with a buffer layer | 3.36 | 2.24 | 1.13 |
| Thermal spraying | 19.48 | 6.44 | 13.04 |
| Post sintering with Ni plates | 6.05 | 3.03 | 3.02 |
| Sputtering | 6.96 | 5.02 | 1.94 |

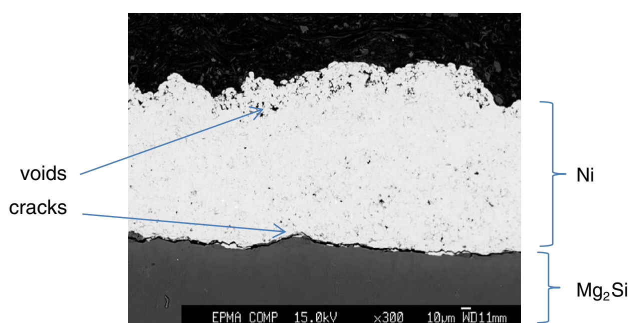


Fig. 5. SEM image of Ni electrode fabricated by thermal spraying.

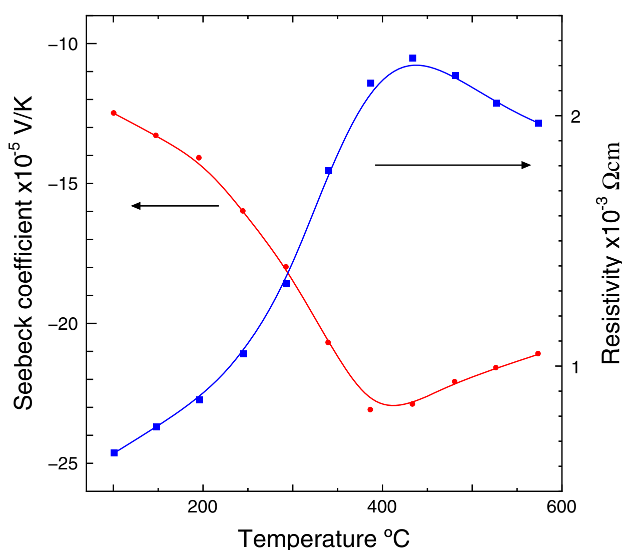


Fig. 6. Temperature dependence of Seebeck coefficient and electrical resistivity.

sputtering, Ni was sputtered on both sides of an $Mg_2Si$ sintered body. The background pressure, sputtering pressure, RF power, and deposition time were $3 \times 10^{-3}$ pa, 0.7 pa, 300 W, and 60 min, respectively. The surface of the $Mg_2Si$ sintered body was etched for 5 min at 300 W before sputtering. Total and contact resistances of devices with buffer layer, thermal spraying, post sintering with Ni plates, and sputtering electrodes are summarized in Table I. This shows that simultaneous sintering with a buffer layer is the best method for electrode fabrication. The resistance of the thermally sprayed electrode is much larger than that of electrodes fabricated by other methods. Cracks between the electrode fabricated by thermal spraying and the $Mg_2Si$ sintered body, and voids in the Ni electrode, are apparent in Fig. 5. We make the conjecture that this is the cause of the high contact resistance. Different Ni film preparation results in different thermal effects on the Ni/$Mg_2Si$ interface. However the best thermal conditions for preparation of low-resistance interfaces are not yet known. More precise study is required to understand the thermal effect on interface resistivity. Figure 6 shows the Seebeck coefficient and resistivity, as a function of temperature, of the device with the electrode prepared by simultaneous sintering with the buffer layer. The highest Seebeck coefficient of $2.3 \times 10^{-4}$ V/K, which is almost same as the value previously obtained,[13] is obtained at approximately 400°C.

## CONCLUSION

For better understanding of $Mg_2Si$ thermoelectric devices, the microstructure of the grain boundary and that of the interface between the electrode and the $Mg_2Si$ sintered body were investigated. We found a boundary layer with a width of a few tens micrometers at the interface which was composed of Ni, Mg, and Si. The electrical resistivity of the layer is as low as that of the Ni electrode. Among the electrode-fabrication methods investigated, simultaneous sintering with the buffer layer was best. Oxygen was detected at the grain boundary of the sintered body but not in the starting materials. This suggests $Mg_2Si$ is oxidized during sintering. It has been reported that the thermoelectric performance of $Mg_2Si$ devices with Ni electrodes deteriorates with time in use.[15] We suspect one of causes of this deterioration is the existence of the boundary layer. We therefore intend to investigate this layer further.

## ACKNOWLEDGEMENTS

This research is partly supported by the Okayama Prefectural Government.

## REFERENCES

1. For example; International Thermoelectric Society Website, Past ICT Details, <http://www.its.org/ict-info>. Accessed 9 Nov 2013.
2. S. Fan, J. Zhao, J. Guo, Q. Yan, J. Ma, and H.H. Hng, *Appl. Phys. Lett.* 96, 182104 (2010).
3. T. Kajikawa, K. Shida, S. Sugihara, M. Ohmori, and T. Hirai, *Proc. ICT'97* (1997), pp. 275–278.
4. S. Battiston, S. Fiameni, M. Saleemi, S. Boldrini, A. Famengo, F. Agresti, M. Stingaciu, M.S. Toprak, M. Fabrizio, and S. Barison, *J. Electron. Mater.* 42, 1956 (2013).
5. C. Nakhowong, T. Sumpao, and T. Seetawan, *Adv. Mat. Res.* 802, 213 (2013).
6. G. Fu, L. Zuo, J. Longtin, C. Nie, and R. Gambino, *J. Appl. Phys.* 114, 144905 (2013).
7. T. Sakamoto, T. Iida, S. Kurosaki, K. Yano, H. Taguchi, K. Nishio, and Y. Takanashi, *J. Electron. Mater.* 40, 629 (2011).
8. T. Sakamoto, T. Iida, A. Matsumoto, Y. Honda, T. Nemoto, J. Sato, T. Nakajima, H. Taguchi, and Y. Takanashi, *J. Electron. Mater.* 39, 1708 (2010).
9. S. Fiameni, S. Battiston, S. Boldrini, A. Famengo, F. Agresti, S. Barison, and M. Fabrizio, *J. Solid State Chem.* 193, 142 (2012).
10. S.-W. You, K.-H. Park, I.-H. Kim, S.-M. Choi, W.-S. Seo, and S.-U. Kim, *J. Electron. Mater.* 41, 1675 (2012).
11. T. Sakamoto, T. Iida, N. Fukushima, Y. Honda, M. Tada, Y. Taguchi, Y. Mito, H. Taguchi, and Y. Takanashi, *Thin Solid Films* 519, 8528 (2011).
12. S. Nakamura, Y. Mori, and K. Takarabe, *ICTMC18, P07-P03*, Salzburg, 27 July–31 Aug. (2012).
13. S. Nakamura, Y. Mori, and K. Takarabe, *Phys. Status Solidi (c)* 10, 1145 (2013).
14. T. Iida, Y. Oguni, and A. Mtsumoto, Japanese Unexamined Patent Application Publication No. 2009-260173.
15. T. Nakamura, K. Hatakeyama, M. Minowa, Y. Mito, K. Arai, T. Iida, and K. Nishio, *ICT2013, P325*, Kobe, 30 June–4 July (2013).